

A trivalent nucleosome interaction by PHIP/BRWD2 is disrupted in neurodevelopmental disorders and cancer

Marc A.J. Morgan,¹ Irina K. Popova,² Anup Vaidya,² Jonathan M. Burg,² Matthew R. Marunde,² Emily J. Rendleman,¹ Zachary J. Dumar,¹ Rachel Watson,² Matthew J. Meiners,² Sarah A. Howard,² Natalia Khalatyan,³ Robert M. Vaughan,⁴ Scott B. Rothbart,⁴ Michael-C. Keogh,² and Ali Shilatifard¹

¹Simpson Querrey Center for Epigenetics, Department of Biochemistry and Molecular Genetics, Northwestern University Feinberg School of Medicine, Chicago, Illinois 60611, USA; ²EpiCypher, Inc., Durham, North Carolina 27709, USA; ³Department of Neurology, Northwestern University Feinberg School of Medicine, Chicago, Illinois 60611, USA; ⁴Department of Epigenetics, Van Andel Research Institute, Grand Rapids, Minnesota 49503, USA

Mutations in the *PHIP/BRWD2* chromatin regulator cause the human neurodevelopmental disorder Chung-Jansen syndrome, while alterations in *PHIP* expression are linked to cancer. Precisely how PHIP functions in these contexts is not fully understood. Here we demonstrate that PHIP is a chromatin-associated CRL4 ubiquitin ligase substrate receptor and is required for CRL4 recruitment to chromatin. PHIP binds to chromatin through a trivalent reader domain consisting of a H3K4-methyl binding Tudor domain and two bromodomains (BD1 and BD2). Using semi-synthetic nucleosomes with defined histone post-translational modifications, we characterize PHIPs BD1 and BD2 as respective readers of H3K14ac and H4K12ac, and identify human disease-associated mutations in each domain and the intervening linker region that likely disrupt chromatin binding. These findings provide new insight into the biological function of this enigmatic chromatin protein and set the stage for the identification of both upstream chromatin modifiers and downstream targets of PHIP in human disease.

[*Keywords:* chromatin; histone; neuroepigenetics; neurodevelopmental disorder]

Supplemental material is available for this article.

Received July 12, 2021; revised version accepted November 9, 2021.

Combinatorial histone modifications recruit multivalent histone binding proteins to orchestrate diverse downstream molecular processes (Kouzarides 2007; Ruthenburg et al. 2007; Musselman et al. 2012). We previously characterized pleckstrin homology interacting protein (PHIP; UniProt Q8WWQ0; also known as BRWD2, RepID, and DCAF14) (Zhang et al. 2016; Morgan et al. 2017; Townsend et al. 2021) as a histone H3 lysine 4 (H3K4) methylation binding protein whose interaction with chromatin is dependent on the COMPASS family of histone H3K4 methyltransferases (Morgan et al. 2017). Loss-of-function mutations in the *PHIP* gene were recently identified as the cause of the neurodevelopmental disorder Chung-Jansen syndrome (Webster et al. 2016; Jansen et al. 2018). PHIP plays a role in an array of biological processes, including cancer pathogenesis (Bezrookove et al. 2018; de Semir et al. 2018, 2020; Weber et al. 2019), cell cy-

cle control (Zhang et al. 2016; Jang et al. 2018, 2020), metabolism (Marenne et al. 2020), and viral infection (Wei et al. 2020). Defining the molecular function of PHIP is of crucial importance to understanding these processes and identifying potential therapeutic targets. The protein domains in PHIP suggest at least two functional activities. The N terminus contains a cullin ring ligase-4 (CRL4) E3 ubiquitin ligase interacting region as well as a series of WD repeats that are characteristic of CRL4 substrate receptors (Angers et al. 2006; He et al. 2006; Higa et al. 2006; Jin et al. 2006; Jang et al. 2018). Toward its C terminus, PHIP contains a cryptic Tudor domain, which binds to histone H3K4 methylation (Morgan et al. 2017), immediately followed by two bromodomains of undetermined function, although other members of this domain family recognize acetylated lysine residues in histone proteins

Corresponding authors: marc.morgan@northwestern.edu, mkeogh@epicypher.com

Article published online ahead of print. Article and publication date are online at <http://www.genesdev.org/cgi/doi/10.1101/gad.348766.121>.

© 2021 Morgan et al. This article is distributed exclusively by Cold Spring Harbor Laboratory Press for the first six months after the full-issue publication date (see <http://genesdev.cshlp.org/site/misc/terms.xhtml>). After six months, it is available under a Creative Commons License (Attribution-NonCommercial 4.0 International), as described at <http://creativecommons.org/licenses/by-nc/4.0/>.

(Kouzarides 2007; Ruthenburg et al. 2007; Musselman et al. 2012). Together, this suggests that PHIP may bind chromatin through multivalent interactions with H3K4 methylation and histone acetylation, and target chromatin-associated substrates for ubiquitination by the CRL4 complex. In support of this notion, CUL4B (a core component of the CRL4 complex) is mutated in Cabezas syndrome, a human neurodevelopmental disorder that shares many features with Chung-Jansen syndrome (Tarpey et al. 2007; Zou et al. 2007).

Here we report several properties of PHIP (BRWD2) that are of considerable biological and pathological interest. We identify PHIP as a chromatin-associated CRL4 substrate receptor, and demonstrate that PHIP is required for the association of CRL4 with chromatin (consistent with recently published data) (Jang et al. 2018). Genetic disruption of all three *PHIP* gene homologs (*BRWD1–3*) results in altered gene expression in cancer cells, which can be partially rescued by re-expression of PHIP. Using semisynthetic nucleosomes with defined histone post-translational modifications (PTMs), we characterize reader activities of the PHIP Tudor and tandem bromodomains (BD1 and BD2). We establish the PHIP BDs as H3K14ac and H4K12ac binding modules and demonstrate a cooperative trivalent nucleosome interaction involving simultaneous binding of H3K4 methylation and these two acetylation sites. Of note, we show that PHIP BD2, which is atypical and contains a threonine in place of the canonical asparagine at the highly conserved acetyl-

lysine binding BC loop, is functional and selective for H4K12ac. We extend the biological relevance of these biochemical experiments by demonstrating that human disease-associated mutations in PHIP impair its ability to bind nucleosomes. These findings provide new insight into the function of this largely uncharacterized chromatin regulator and have implications for the study of human neurodevelopment, cancer biology, and metabolism.

Results

PHIP is a chromatin-associated CRL4 substrate receptor

The CRL4 E3 ubiquitin ligase complex (CUL4A/B, DDB1, and RBX1) forms complexes with dozens of substrate receptors, including PHIP, to target diverse substrates for ubiquitination (Petroski and Deshaies 2005; Angers et al. 2006; He et al. 2006; Higa et al. 2006; Jin et al. 2006; Lydeard et al. 2013). We examined PHIP and CRL4 colocalization by subcellular fractionation (Fig. 1A), and observed that PHIP is almost exclusively in the chromatin fraction, whereas CRL4 is detected across all fractions (Fig. 1A). Notably, chromatin-associated CRL4 is enriched for the active primarily Nedd8-modified form (Petroski and Deshaies 2005; Lydeard et al. 2013), detected by mobility shift on SDS-PAGE. We next examined the repertoire of CRL4 substrate receptor interactions in each fraction. To accomplish this, we cross-linked cells with dithiobis(succinimidyl propionate) (DSP) prior to cell lysis

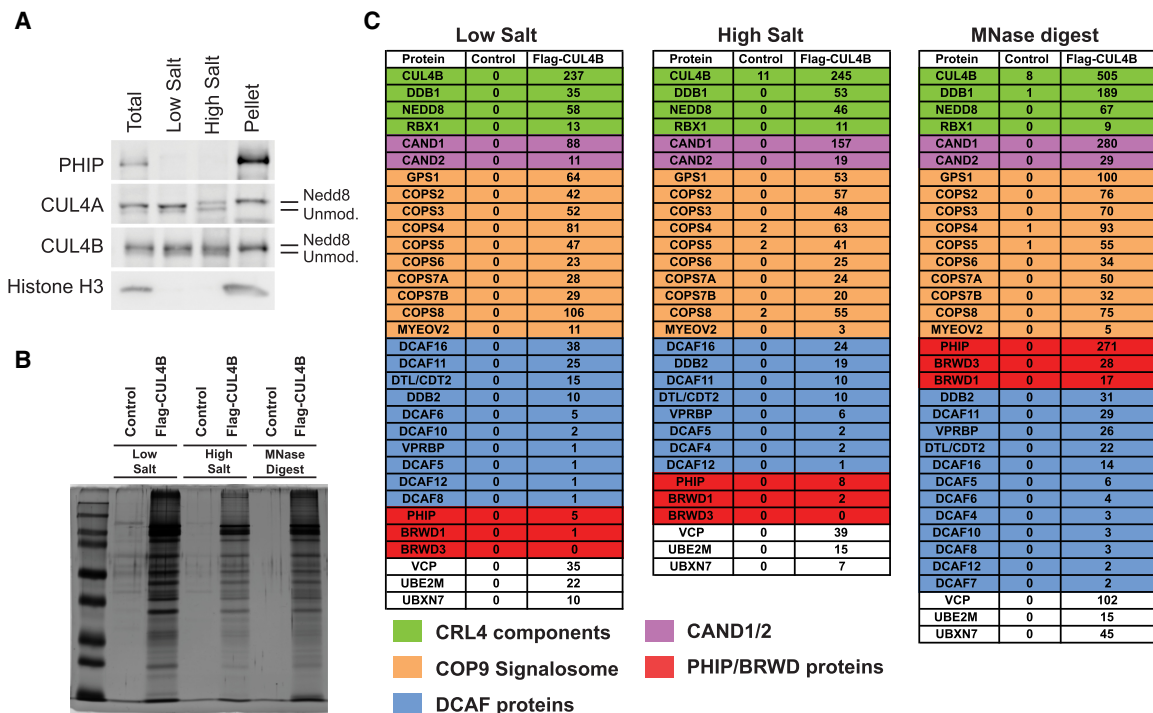


Figure 1. PHIP is the major chromatin-associated CRL4 substrate receptor. (A) Immunoblotting of subcellular fractions from HCT116 cells probed with the antibodies indicated. Nedd8-modified and unmodified CUL4A/B bands are indicated. (B) Silver-stained SDS-PAGE of anti-FLAG immunoprecipitations from control or FLAG-CUL4B-expressing T-Rex-293 cells. (C) Mass spectrometry (MS) spectral counts of FLAG-CUL4B-associated proteins in subcellular fractions.

to limit *in vitro* substrate receptor exchange (Reitsma et al. 2017). We then immunoprecipitated CRL4 through a FLAG-tagged CUL4B subunit and performed mass spectrometry (MS) analysis of protein complexes (Fig. 1B,C). CRL4–PHIP complexes are more abundant in micrococcal nuclease [MNase]-digested chromatin relative to the low- and high-salt fractions (Fig. 1C), suggesting that PHIP interacts with CRL4 specifically on chromatin.

Given their physical interaction, we next examined whether *PHIP/BRWD2*, or its close homologs *BRWD1* and *BRWD3*, are individually required for CRL4 association with chromatin. Individual elimination of *BRWD1* and *BRWD3* has minimal effect on CRL4 chromatin binding, although it is diminished on deletion of *PHIP* (Fig. 2A), as reported recently (Jang et al. 2018). To uncover po-

tential redundancy between the homologs, we engineered *BRWD1/2/3* triple gene knockout (BRWD TKO) cells (Fig. 2B) and observed markedly decreased proliferation (Fig. 2C) and dramatically reduced CRL4 binding to chromatin (Fig. 2D). We next characterized the chromatin-associated proteome of BRWD TKO cells by performing quantitative tandem mass tag (TMT) MS, confirming that CRL4 is depleted from chromatin (Fig. 2E).

PHIP regulates gene expression in cancer cells

To gain further insight into the role of PHIP, we performed global mRNA profiling in control and BRWD TKO cells and observed gene expression alterations (Fig. 3A). To determine to what extent these changes are direct effects

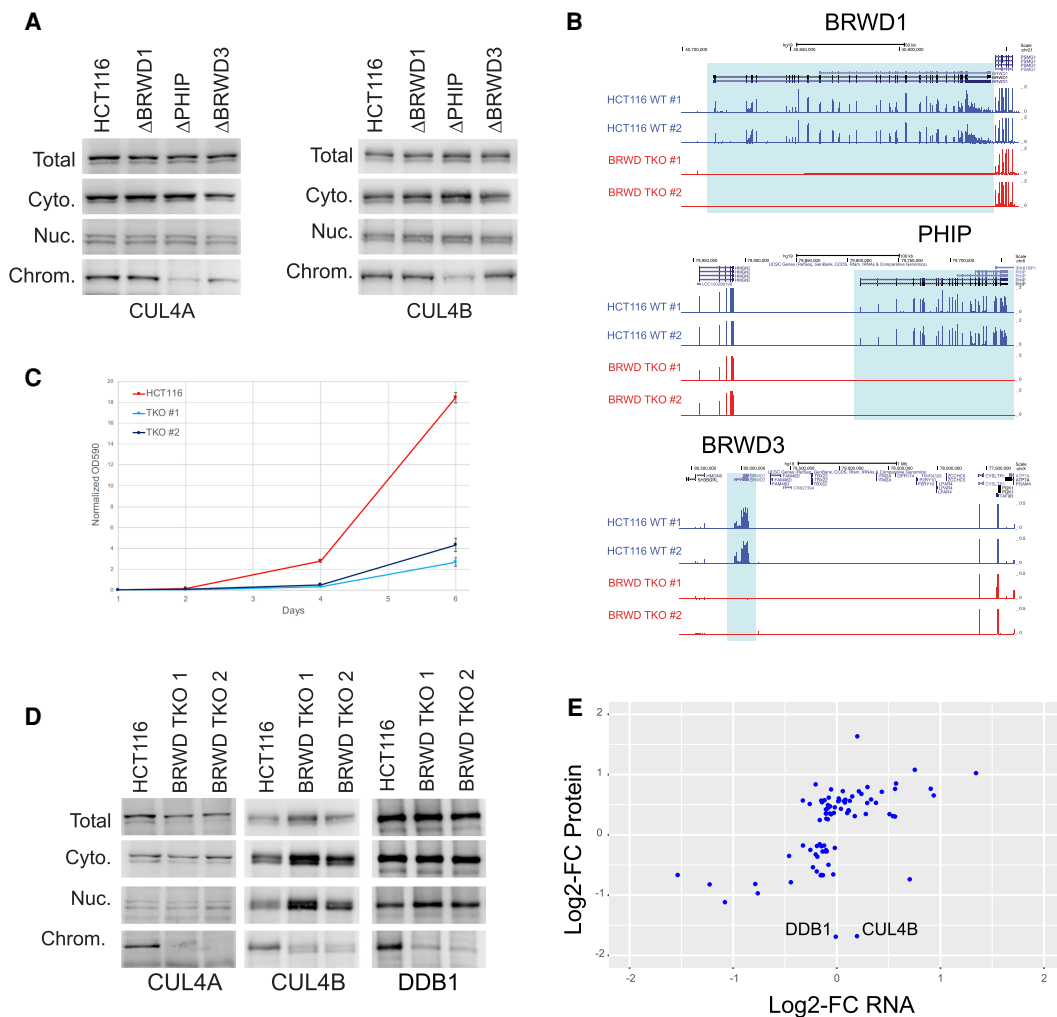


Figure 2. PHIP is required for CRL4 association with chromatin. (A) Immunoblotting of subcellular fractions from wild-type and BRWD1, BRWD2, and BRWD3 knockout HCT116 cells probed for the CRL4 components CUL4A (left) and CUL4B (right). (B) RNA sequencing tracks from wild-type and BRWD triple knockout (BRWD TKO) cells confirming disruption of all three genes. (C) Crystal violet-staining cell growth assay of wild-type and BRWD TKO cells. (D) Immunoblotting of subcellular fractions from wild-type and BRWD TKO cells probing for CRL4 components, CUL4A (left), CUL4B (middle), and DDB1 (right). (E) Tandem mass tag (TMT) MS analysis of chromatin-associated proteins in wild-type and BRWD TKO cells. TMT data were integrated with RNA-seq data and are presented as log₂ fold change in RNA plotted against log₂ fold change in protein. RNA levels for the CRL4 components CUL4B and DDB1 were unchanged, whereas their proteins were dramatically depleted from chromatin.

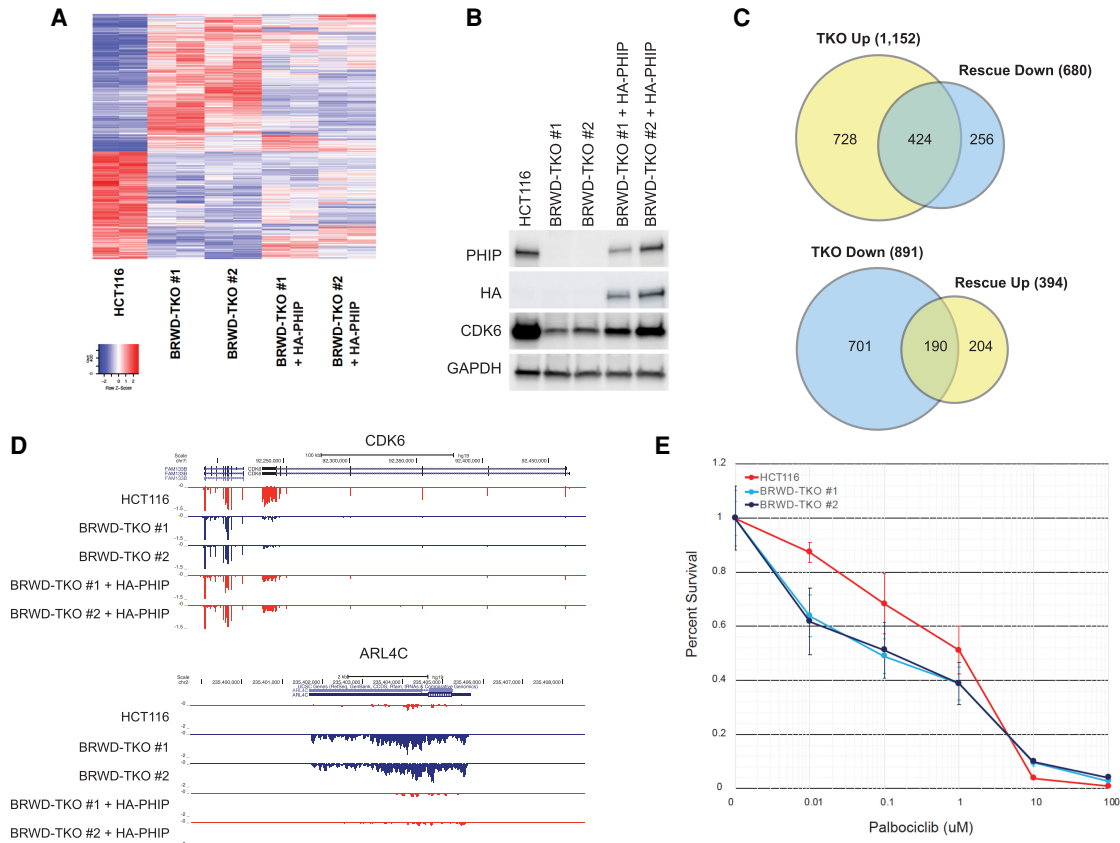


Figure 3. PHIP regulates gene expression in cancer cells. (A) RNA sequencing heat map plotting wild-type, BRWD TKO, and HA-PHIP-rescued cells. The gene sets displayed are those differentially expressed between wild-type and BRWD TKO cells. (B) Immunoblotting of whole-cell extracts from wild-type, BRWD TKO, and PHIP-rescued cells probed with the antibodies indicated. (C) Venn diagrams displaying genes in BRWD TKO that increase or decrease toward wild-type levels upon PHIP re-expression. (D) UCSC genome browser RNA-seq track examples of a BRWD TKO down-regulated gene (CDK6) that is up-regulated upon PHIP re-expression (*top*) and a BRWD TKO up-regulated gene (ARL4C) that is decreased upon PHIP re-expression (*bottom*). (E) Crystal violet cell growth assay of wild-type and BRWD TKO cells treated with palbociclib for 48 h.

of *PHIP* gene deficiency, we re-expressed HA-tagged PHIP in BRWD TKO cells using a lentiviral vector (Fig. 3A,B) and observed that ~36% of up-regulated genes and ~21% of down-regulated genes are at least partially restored (Fig. 3C), suggesting that PHIP may mediate an activating or repressive role. Notably, cell cycle regulator cyclin-dependent kinase 6 (CDK6) levels (mRNA and protein) were dramatically reduced in BRWD TKO cells and partially restored upon PHIP rescue (Fig. 3B,D). BRWD TKO cells also appear more sensitive to low doses of the CDK4/6 inhibitor, palbociclib (Fig. 3E), while previous work identified a role for PHIP in promoting Cyclin D1 expression in triple-negative breast cancer cells (de Semir et al. 2018). Taken together, this suggests that PHIP may regulate G1/S CDK4/6-CyclinD activity in transformed cells.

Phip is dispensable for neurogenesis

To investigate the role of *PHIP* in developmental processes, we used a mouse embryonic stem cell (ESC)-based differentiation system. We derived multiple *PHIP* knockout

ESC lines (Supplemental Fig. S1A) and subjected these to in vitro cortical neuronal differentiation (Gaspard et al. 2009), followed by immunohistochemical analysis and RNA sequencing. *PHIP*-null ESCs are capable of forming both neuronal progenitors and fully differentiated neurons, as demonstrated by immunostaining for Nestin and TUBB3, respectively (Supplemental Fig. S1B). Transcriptome analysis indicates that *PHIP* knockout results in minimal alterations in gene expression in undifferentiated ESCs and neuronal cultures (Supplemental Fig. S1C–E). These results are in line with the published phenotype of *PHIP* mutant mice, which appear grossly normal at birth but exhibit postnatal lethality within the first month of life (Li et al. 2010). This implies that *PHIP* is not essential for early embryonic development but has a crucial function for postnatal survival.

The *PHIP* bromodomains engage H3K14ac and H4K12ac

To further explore the mechanisms of PHIP-mediated recruitment of CRL4 to chromatin, we turned our attention

to the PHIP chromatin binding region (residues 940–1434), containing a Tudor domain immediately upstream of tandem bromodomains (referred to here as BD1 and BD2). Our previous work characterized the Tudor domain as a H3K4 methylation reader (Morgan et al. 2017). However, direct evidence for PHIP bromodomain binding to specific histone PTMs is lacking. Therefore, we initially performed a histone-peptide microarray screen using a recombinant construct containing the Tudor and tandem BDs with an N-terminal 10x-histidine tag (Tudor–BD1–BD2). In addition to the expected H3K4 methyl peptides, this identified those containing multiple sites of histone H3 and H4 N-terminal tail acetylation as candidate binding sites (Supplemental Fig. S2).

To quantitatively interrogate PHIP binding and refine the candidate interactions with a physiological target, we performed dCypher assays using semisynthetic PTM-defined nucleosomes (Weinberg et al. 2019; Jain et al. 2020; Marunde et al. 2021). For these experiments, we used the wild-type Tudor–BD1–BD2 construct above as well as versions harboring mutations that would be expected to abrogate the PTM-binding function of each individual domain: Tudor^{Mut}; W1081A, BD1^{Mut}; N1239A, and BD2^{Mut}; T1396A (Fig. 4A; Filippakopoulos et al. 2012; Morgan et al. 2017). We initially measured wild-type binding to H3K4 methylated nucleosomes and observed a marked preference for H3K4me3/2 over H3K4me1 (Fig. 4B,C). Importantly, this binding was ablated by Tudor^{Mut} but unaffected by BD1^{Mut}–BD2^{Mut} (Fig. 4B,C), demonstrating that the Tudor domain is both necessary and sufficient for binding to H3K4 methylation in a nucleosomal context.

Whereas PHIP BD1 has a canonical BC-loop sequence with an asparagine (N1239) at the acetyl-lysine binding position, BD2 is atypical with a threonine (T1396) at this location, raising the possibility that BD2 is nonfunctional. To explore their capability and specificity, we assayed PHIP BD1^{Mut} and BD2^{Mut} against a panel of PTM-defined nucleosomes containing individual or combinatorially

acetylated lysines on histone H3 (K4, K9, K14, and K18), H4 (K5, K8, K12, and K16), and H2A (K5, K9, K13, and K15). Consistent with results from histone peptide arrays (Supplemental Fig. S2), wild-type PHIP bound H3 and H4 tetra-acetylated (tetraAc) nucleosomes, but also those containing only H3K14ac or H4K12ac (Fig. 4D,E). Notably, binding affinity was increased when nucleosomes contained both tetra-acetylated H3 and H4, suggesting multivalent *trans*-tail engagement with H3K14ac and H4K12ac. Supporting this idea, BD1^{Mut} eliminates binding to H3K14ac and H3tetraAc nucleosomes, but retains binding to H4K12ac and H4tetraAc nucleosomes (Fig. 4D,E). Conversely, BD2^{Mut} loses binding to H4K12ac and H4tetraAc nucleosomes, but retains binding to H3K14 and H3tetraAc nucleosomes (Fig. 4D,E). In each BD mutant form, the enhanced binding observed by combining H3 and H4tetraAc nucleosomes is lost. Thus, PHIP BD1 and BD2 bind to H3K14ac and H4K12ac, respectively, and the presence of both PTMs enhances nucleosome engagement.

To examine the distribution of these histone PTMs in a cellular context, we performed ChIP-seq for each (H3K4me1, H3K4me2, H3K4me3, H3K14ac, and H4K12ac) and PHIP in HCT116 cells and observed extensive colocalization of all tested elements (Fig. 5A). As we previously reported, PHIP occupies gene promoters with high levels of H3K4me3 as well as intergenic putative enhancers marked by H3K4me1 (Fig. 5B). Analysis of ChIP-seq peak overlaps demonstrates that PHIP binding co-occurs with combinations of H3K4 methylation, H3K14ac, and H4K12ac (Fig. 5C,D). Collectively, these experiments strongly suggest that a combination of H3K4 methylation, H3K14ac, and H4K12ac creates high-affinity binding sites for PHIP and promotes its chromatin occupancy.

PHIP forms a trivalent interaction with nucleosomes

We next further examined the role of combinatorial histone PTMs in regulating PHIP nucleosome binding. To

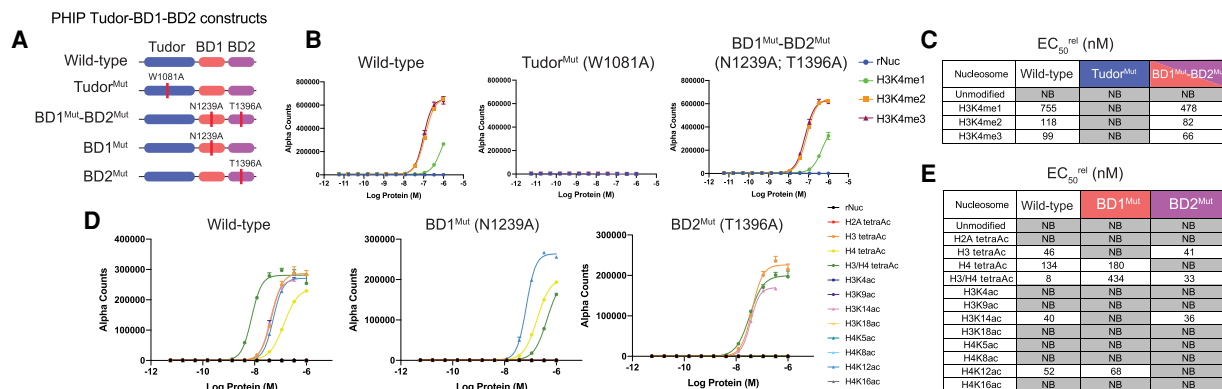


Figure 4. The PHIP bromodomains bind nucleosomal H3K14ac and H4K12ac. (A) Diagram of PHIP Tudor–BD1–BD2 constructs used in binding studies indicating the locations of point mutations. (B) dCypher nucleosome binding assays using wild-type (left), Tudor^{Mut} (middle), and BD1^{Mut}–BD2^{Mut} mutant (right) constructs in combination with the H3K4 methylation-containing nucleosomes indicated. (C) Table of EC₅₀^{rel} values for the experiments shown in B. (D) dCypher nucleosome binding assays using wild-type (left), BD1^{Mut} (middle), and BD2^{Mut} (right) in combination with the acetylation-containing nucleosomes indicated. (E) Table of EC₅₀^{rel} values for the experiments shown in D. [NB] No binding.

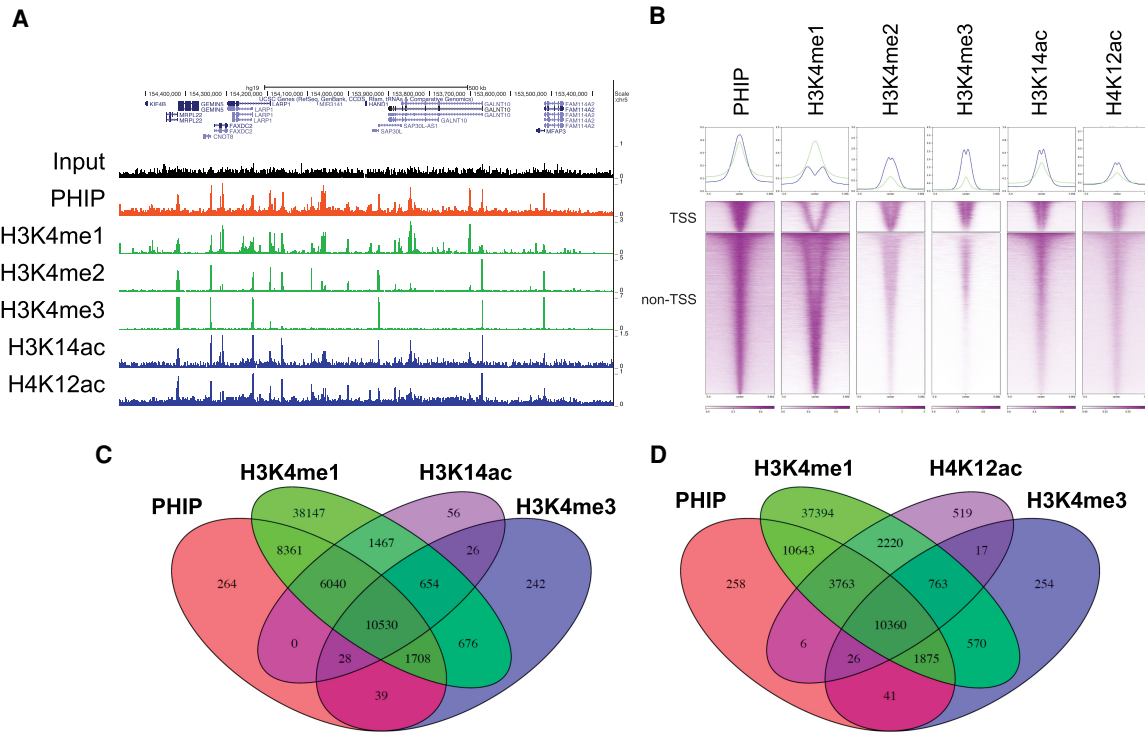


Figure 5. PHIP colocalizes with H3K4 methylation, H3K14ac, and H4K12ac on chromatin. (A) UCSC genome browser ChIP-seq track example for ChIPs of PHIP, H3K4me1, H3K4me2, H3K4me3, H3K14ac, and H4K12ac. (B) Heat map of ChIP-seq data centered on PHIP peaks. Peaks were divided into transcription start sites (TSSs) and non-TSS peaks. (C) Venn diagram displaying overlapping ChIP-seq peaks for PHIP, H3K4me3, H3K4me1, and H3K14ac. (D) Venn diagram displaying overlapping ChIP-seq peaks for PHIP, H3K4me3, H3K4me1, and H4K12ac.

achieve this, we generated nucleosomes containing H3K4 methylation in combination with H3K14ac or H4K12ac. When H3K4 methylation is combined with H3K14ac, there is an increase in PHIP binding affinity that is disrupted by Tudor^{Mut} or BD1^{Mut} (Fig. 6A,B). As above, wild-type PHIP prefers H3K4me2/3 over H3K4me1 in the absence of combinatorial acetylation (Fig. 4B,C). However, when H3K14ac is present, there is minimal difference in affinity for these three H3K4 methylation states (Fig. 6A,B). This observation is consistent with our ChIP-seq results, which show that PHIP occupies many genomic regions that are marked by H3K4me1 but have low levels of H3K4me2/3 (Fig. 5), and suggests that co-occurrence of H3K14ac may promote binding at these sites. Similar to H3K14ac, H4K12ac enhances wild-type PHIP interaction with nucleosomes when combined with H3K4 methylation. However, distinct from H3K14ac, there is still a detectable difference in binding between H3K4me1 and H3K4me3/2 in combination with H4K12ac (Fig. 6C,D).

Standard dCypher assay conditions titrate varying concentrations of Query (e.g., Tudor-BD1-BD2) into a fixed concentration of Target (e.g., a PTM-defined nucleosome) (Marunde et al. 2021). In this setup, we were able to detect enhanced binding of wild-type PHIP with all pairwise PTM combinations engaged by its Tudor (H3K4methyl), BD1 (H3K14ac), and BD2 (H4K12ac), but were not able to distinguish any increase in binding with all three PTMs,

potentially due to saturation of the assay signal (Supplemental Fig. S3). To overcome this, we modified the dCypher assay by moving to a fixed low concentration of wild-type PHIP (reduced 400-fold from typical) and titrating in PTM-defined nucleosomes (see the Materials and Methods). This revealed increased binding to a triple-PTM nucleosome (H3K4me3, H3K14ac, and H4K12ac) relative to each combination of two PTMs (Fig. 6E,F). As an additional control, we titrated the triple-PTM nucleosomes against wild-type and mutant PHIP constructs, and determined that mutation of any individual domain (Tudor^{Mut}, BD1^{Mut}, or BD2^{Mut}) decreased binding (Fig. 6G,H).

We next explored cooperative histone binding in a cellular context by generating cells with a deletion of both bromodomains using CRISPR-Cas9 gene editing of endogenous PHIP in HCT116 cells. To achieve this, we introduced sgRNAs targeting PHIP intronic sequences to create a 16-kb deletion that causes in-frame splicing between exon 30 and exon 39 and encodes a protein retaining the Tudor domain but lacking both bromodomains (PHIP Δ Bromo) (Fig. 6I). After subcellular fractionation (see the Materials and Methods), wild-type PHIP is primarily found in the chromatin fraction (as expected) (Fig. 1A), while PHIP Δ Bromo is detectable in the soluble and chromatin pools, suggesting diminished chromatin binding (Fig. 6J). We next used ChIP-seq to compare the

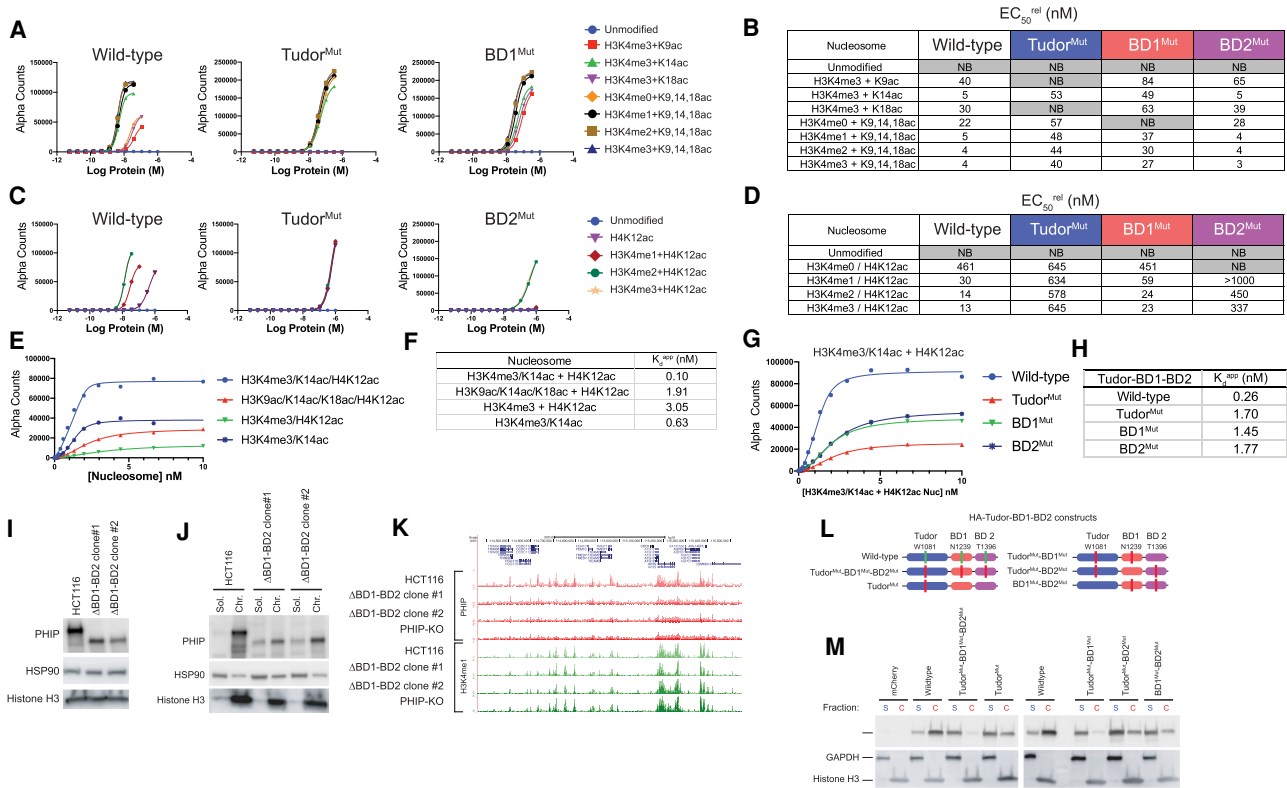


Figure 6. PHIP forms a trivalent nucleosome interaction. (A) dCypher nucleosome binding assays using wild type (left), Tudor^{Mut} (middle), and BD1^{Mut} (right) and the panel of nucleosomes indicated. (B) Table of EC₅₀^{rel} values for the experiments shown in A. (C) dCypher nucleosome binding assays using PHIP wild type (left), Tudor^{Mut} (middle), and BD2^{Mut} (right) using the panel of nucleosomes indicated. (D) Table of EC₅₀^{rel} values for the experiments shown in C. (NB) No binding. (E) Modified dCypher assay (Target depletion/Query limited conditions) using the wild-type construct in combination with the nucleosomes indicated. (F) Table of K_d^{app} values for the experiments presented in E. (G) Modified dCypher assays performed with wild-type, Tudor^{Mut}, BD1^{Mut}, and BD2^{Mut} constructs in combination with H3K4me3/H3K14ac + H4K12ac nucleosomes. (H) Table of K_d^{app} values for the experiments presented in G. (I) Immunoblotting of whole-cell extracts from wild-type cells and two independent clones of PHIP ΔBD1–BD2 HCT116 cells. (J) Immunoblotting of subcellular fractions from wild-type and ΔBD1–BD2 cells. (K) UCSC genome browser ChIP-seq track example of ChIP experiments performed in wild-type, ΔBD1–BD2, and PHIP KO cells using antibodies directed against PHIP and H3K4me1. (L) Diagram of the PHIP Tudor bromodomain lentiviral constructs used in subcellular fractionation experiments. (M) Immunoblotting of soluble (S) and chromatin (C) fractions from cells expressing the constructs shown in L. GAPDH and histone H3 serve as protein markers for the soluble and chromatin fractions, respectively.

genome-wide binding of PHIP wild type and ΔBromo relative to PHIP KO, which revealed reduced signal in the mutant that was comparable with the background levels of KO cells (Fig. 6K). This is consistent with dCypher data, and suggests that multiple interactions are required for high-affinity binding of PHIP to chromatin, and the Tudor domain alone is insufficient to drive normal chromatin localization in vivo. As a further test of this model, we generated lentiviral HA-tagged full-length PHIP constructs encoding wild type, single mutations, or combinations of Tudor^{Mut}, BD1^{Mut}, and BD2^{Mut} (Fig. 6L). We stably expressed these constructs in mammalian cells and performed subcellular fractionation followed by immunoblotting, and observed that while wild-type protein is primarily detected in the chromatin fraction, mutation of each PTM interaction domain resulted in a shift to the soluble fraction (Fig. 6M). The most dramatic effect was seen on simultaneous mutation of all three reader do-

main, Tudor^{Mut}-BD1^{Mut}-BD2^{Mut}, closely followed by Tudor^{Mut}-BD1^{Mut} (Fig. 6M).

PHIP chromatin binding is disrupted in neurodevelopmental disorders and cancer

To explore the potential role of PHIP chromatin binding activity in human disease, we assembled a panel of chromatin binding region mutations that have been detected in human neurodevelopmental disorders or cancer (Fig. 7A; Firth et al. 2009; Jansen et al. 2018; Tate et al. 2019; Tenorio et al. 2019; van der Donk et al. 2019; McLeod et al. 2021). These mutations involved the Tudor domain (E963G and W1156L), BD1 (Q1263E), BD2 (R1402S), and the linker between BD1 and BD2 (R1310C). In dCypher testing, E963G and Q1263E had no discernible impact, which may reflect sensitivity limitations of the approach under standard conditions (Supplemental Fig. S4).

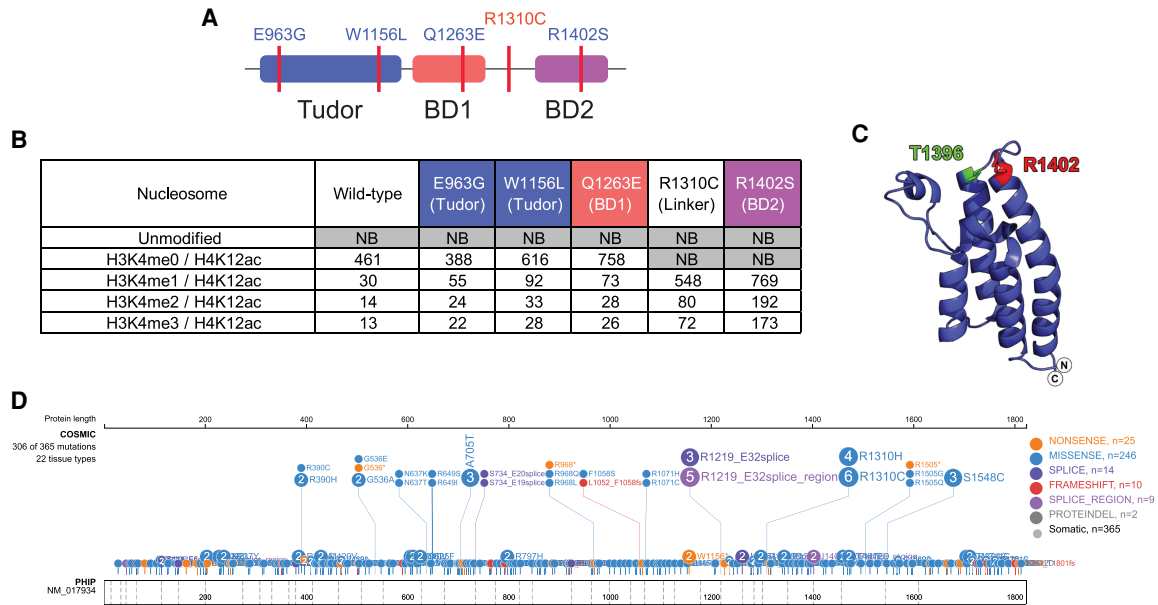


Figure 7. PHIP nucleosome binding is disrupted in human disease. (A) Diagram of the PHIP mutations associated with human developmental disorders (blue text) or cancer (red text) located within the chromatin binding domain. (B) Table of EC_{50}^{rel} values for wild type and the disease-associated PHIP mutations shown in A against the nucleosomes indicated. (NB) No binding. (C) Location of the R1402 residue, highlighted in red, on the structure of PHIP bromodomain 2 (PDB: 3MB3); the acetyl binding position T1396 is highlighted green. (D) Pe-Can plot (St. Jude Cloud) of PHIP displaying cancer-associated mutations from the COSMIC database.

However, W1156L (within Tudor domain) showed reduced binding (more than threefold relative to wild type) to H3K4me1-2/H4K12ac nucleosomes, while R1402S (within BD2) had a dramatic impact (>10-fold reduced binding relative to wild type) for nucleosomes containing the H3K4 methyl states and H4K12ac, suggesting defective BD2 function (Fig. 7B). In the PHIP BD2 crystal structure (PDB: 3MB3) (Filippakopoulos et al. 2012), R1402S is located at the beginning of the B helix in close proximity to the acetyl-lysine binding site (Fig. 7C), and our experiments demonstrate that this position contributes directly to Kac binding. Perhaps the most intriguing impact was observed from R1310C (the most frequent PHIP mutation detected in human cancer), with more than fourfold reduced binding relative to wild type toward H3K4me1-2/H4K12ac nucleosomes (Fig. 7B,D). Intriguingly, this mutation in the linker between BD1 and BD2 specifically compromises function of the latter (binding to H4K12ac), indicating the importance of flanking regions to the minimal reader domains, and the necessity to study these elements in context. Collectively these results implicate disruption of PHIP chromatin binding in cancer and neurodevelopmental disorders.

Discussion

Defining the molecular functions of PHIP (BRWD2) will provide insight into the diverse processes it controls, such as neurodevelopment, metabolism, and cancer pathogenesis. Here we demonstrate that PHIP is a chromatin-associated CRL4 substrate receptor, and that its loss

impairs CRL4 interaction with chromatin. Deletion of the three *BRWD* gene homologs (*BRWD1-3*) results in altered gene expression in human cancer cells that can be partially rescued by *PHIP* re-expression. We have extensively characterized PHIP chromatin binding activity and defined the means by which it interacts with PTM-defined nucleosomes. Building on our previous findings identifying the PHIP Tudor domain as a H3K4 methyl binding module, we demonstrate that BD1 and BD2 mediate interaction with H3K14ac and H4K12ac (Fig. 8). Finally, we extend the in vivo relevance of these biochemical studies by identifying human disease-associated mutations within the PHIP chromatin binding domain that impair its ability to bind nucleosomes.

By individually deleting each of the three *BRWD* gene homologs, we have shown that *PHIP* is of primary importance for the association of CRL4 with chromatin, a finding in line with recent work (Jang et al. 2018). In our TMT MS and analysis of immunoprecipitated CRL4 complexes, we observed that PHIP is the most abundant of the three *BRWD* homologs in HCT116 cells, providing the simplest explanation for its contribution to CRL4 recruitment. However, we note the distinct loss-of-function phenotypes for *BRWD1*, *PHIP* (*BRWD2*), and *BRWD3*, indicating nonredundant functions and/or different patterns of expression. In this manner, *BRWD1* is essential for normal germ cell development and mediates immunoglobulin gene rearrangement (Philipps et al. 2008; Mandal et al. 2015). *PHIP* mutant mice exhibit postnatal lethality (Li et al. 2010), while human haploinsufficiency causes Chung-Jansen syndrome (Webster et al. 2016; Jansen et al. 2018). Finally, loss-of-function mutations in human

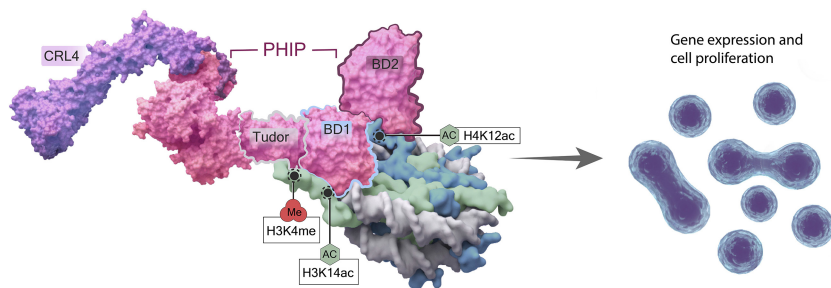


Figure 8. Summary figure of PHIP nucleosome binding and molecular function. PHIP interacts with trivalent (H3K4me/H3K14ac/H4K12ac) nucleosomes to recruit the CRL4 complex to direct gene expression and drive cellular proliferation.

BRWD3 result in an X-linked intellectual disability syndrome (Field et al. 2007).

Precisely how the PHIP–CRL4 complex functions in cellular biology is not fully understood. Mutations in human PHIP and CRL4 cause phenotypically similar neurodevelopmental disorders, so direct targets for PHIP–CRL4 ubiquitin ligase activity are likely of disease relevance. In addition to potential roles regulating gene expression by binding histones PTMs associated with active chromatin (Morgan and Shilatifard 2020), a growing body of literature links PHIP–CRL4 to DNA replication and other aspects of cell cycle control. PHIP binds a subset of DNA origins of replication and is required for initiation at these sites (Zhang et al. 2016; Jang et al. 2018). It also plays a role in the response to DNA replication stress by stabilizing stalled replication forks (Townsend et al. 2021). In addition, PHIP functions during mitosis by acting as a scaffold to transfer CRL4 to RBBP7, which mediates the degradation of BUB3 to regulate the metaphase-to-anaphase transition (Jang et al. 2020). Thus, PHIP may have a number of roles related to diverse aspects of chromatin function, and it will be important to investigate how its histone PTM engagement regulates these processes.

Our characterization of the PHIP chromatin binding module as a trivalent (H3K4 methyl, H3K14ac, and H4K12ac) reader has implications with respect to PHIP recruitment to chromatin and the development of molecules targeting its activity. Bromodomains have been grouped into eight classes based on amino acid sequence and structural data (Filippakopoulos et al. 2012). The vast majority contain an asparagine residue at the acetyl-lysine binding position located at the end of the Ba helix, immediately preceding the B–C loop (Filippakopoulos et al. 2012). Most bromodomains share a common overall fold but exhibit significant amino acid diversity/divergence in the distribution of charged surface residues, which most likely contributes to substrate specificity (Filippakopoulos et al. 2012). PHIP BD1 falls within bromodomain class VII, which includes TAF1, ZMYND8, and ZMYND11. TAF1 bromodomains recognize multiple acetylated histone H4s (Jacobson et al. 2000; Flynn et al. 2015), whereas ZMYND8 interacts with H3K14ac (Li et al. 2016; Savitsky et al. 2016), in common with PHIP BD1 (Fig. 4D,E), suggesting that these domains may constitute a related subfamily. PHIP BD2 is atypical (containing a threonine residue at the acetyl-lysine binding position), and falls within bromodomain class III, which also includes the bromodomains of the acetyltransferases

CBP and p300 (Filippakopoulos et al. 2012). The CBP bromodomain contains a canonical asparagine acetyl-lysine binding residue and strongly interacts with H3K56ac but is also capable of binding the diverse targets H3K36ac, H3K79ac, H4K12ac, and H4K44ac (Picaud et al. 2015). When tested to a limited number of these potential targets in the nucleosome context, PHIP BD2 shows specific interaction with H4K12ac, suggesting that although it shares structural similarity with CBP, it may possess a distinct histone binding activity. Outside the three BRWD homologs, the only other annotated bromodomain with a threonine at the acetyl-lysine binding position is TRIM28, though this bears little resemblance to PHIP BD2 outside of the acetyl-lysine binding site (Filippakopoulos et al. 2012). The TRIM28 bromodomain has been suggested to lack acetyl-lysine binding activity (Zeng et al. 2008), though our demonstration of PHIP BD2 functionality suggests it may be worth re-examining this prediction. Intriguingly, a recent study identified PHIP BD2 as capable of binding both formyl- and propionyl-lysine (Flynn et al. 2015), though this activity was not mapped to a specific histone residue. Our identification of R1402 as being critical for PHIP BD2 function provides insight into the impact of this mutation in human neurodevelopmental disorders. However, the observation that mutation of R1310 in the linker region preceding BD2 impairs its ability to bind H4K12ac may have the greatest resonance outside this study. It is likely that “minimal domain/histone peptide” interrogations have dramatically underappreciated the complexity of the interactions (and their means of regulation) between full-length reader proteins and their nucleosome targets. Working with a more physiological representation of the potential interacting partners will almost certainly uncover additional regulatory regions and the mechanism of disease alleles.

Our dCypher and ChIP-seq experiments suggest that H3K4 methyl, H3K14ac, and H4K12ac nucleosomes serve as high-affinity PHIP binding sites, implying a concerted activity of COMPASS methyltransferases and lysine acetyltransferases, and understanding how this is coordinated will be an important area for future work. Potential candidates involved in recruiting PHIP to H3K14ac include GCN5 and HBO1, while HAT1 and NuA4 may mediate H4K12ac (Roth et al. 2001; Lee and Workman 2007; Kueh et al. 2020).

PHIP is overexpressed in many cancers and acts as a potential regulator of their proliferation (De Semir et al. 2012, 2018, 2020; Zhang et al. 2016; Bezrookove et al. 2018; Jang

et al. 2018, 2020; Weber et al. 2019), suggesting that the development of small molecules targeting PHIP chromatin binding could be a useful therapeutic. Indeed, efforts have already been made to develop an inhibitor of PHIP BD2 function (Cox et al. 2016). Recent studies have demonstrated that targeting a single reader domain in a multivalent chromatin protein can be sufficient to disrupt normal localization (Dilworth et al. 2021). Thus, our characterization of the substrate specificity of each reader domain in PHIP may open up additional approaches to target its function.

The characterization of the methylation and acetylation pathways that control PHIP recruitment to chromatin have important implications for the development of targeted treatments for Chung-Jansen syndrome. Here, affected individuals carry heterozygous de novo loss-of-function mutations in *PHIP* (Webster et al. 2016; Jansen et al. 2018), so it is plausible that increasing the functional activity of the remaining wild-type protein could alleviate disease symptoms. One approach to achieve this would be small molecule inhibitors directed toward the activity of enzymes that remove the H3K4 methyl and H3K14ac/H4K12ac PTMs. Indeed, such an approach has already proven fruitful in the case of *MLL4/KMT2D*, which is heterozygously mutated in the neurodevelopmental Kabuki syndrome (Bjornsson et al. 2014; Zhang et al. 2021). *MLL4/KMT2D* is a member of the COMPASS family of methyltransferases that acts on H3K4 and also promotes histone acetylation through association with KDM6A/UTX (Wang and Shilatifard 2019). Recent studies in the context of *MLL4* haploinsufficiency have demonstrated that increasing acetylation by blocking histone deacetylase activity (Bjornsson et al. 2014), or increasing H3K4 methylation by inhibiting LSD1/KDM1A demethylase (Zhang et al. 2021), can rescue features of a mouse model of Kabuki syndrome. Thus, modulating enzymatic activity to promote the recruitment of PHIP to chromatin could have a therapeutic impact in Chung-Jansen syndrome.

Materials and methods

Cell culture

HCT116 and HEK293T cells were from ATCC and grown in Dulbecco's modified Eagle's medium (DMEM) supplemented with 15% fetal bovine serum, 2 mM L-glutamine, 1× MEM nonessential amino acids, and penicillin/streptomycin. Cell lines were evaluated for the presence of mycoplasma by RNA sequencing.

Plasmids

CRISPR sgRNA constructs (Supplemental Table 1) were ordered as complementary oligonucleotides (Integrated DNA Technologies [IDT]), annealed, and cloned into pX330-U6-Chimeric_BB-CBh-hSpCas9. pSin-HA-PHIP was constructed by subcloning a full-length PHIP-coding sequence (Morgan et al. 2017) into a modified version of pSin-EF2-Puro containing an N-terminal HA tag. For *E. coli* expression, PHIP-coding sequences (Supplemental Table 1) were synthesized by IDT and cloned into pET16b (Millipore Sigma 69662) using HiFi DNA assembly master mix (New England Biolabs E2621L). FLAG-tagged CUL4B was PCR-amplified using the

pcDNA3-myc3-CUL4B plasmid as template and cloned into pcDNA5/FRT/TO (Thermo Fisher V652020). pX330-U6-Chimeric_BB-CBh-hSpCas9 was a gift from Feng Zhang (Addgene 42230) (Cong et al. 2013). pcDNA3-myc3-CUL4B was a gift from Yue Xiong (Addgene 19922) (Hu et al. 2008). pSin-EF2-Oct4-Pur was a gift from James Thomson (Addgene 16579) (Yu et al. 2007). pMD2.G was a gift from Didier Trono (Addgene 12259). psPAX2 was a gift from Didier Trono (Addgene 12260). pCAGGS-EGFP-IRES-Puro was a gift from Dr. Hitoshi Niwa.

Lentivirus preparation

HEK293T cells were plated at 6×10^6 cells per 10-cm dish and transfected the following day using 10 μ g of lentiviral transfer plasmid, 8 μ g of psPAX2 (Addgene 12260), 4 μ g of pMD2.G (Addgene 12259), and 44 μ g of polyethylenimine (PEI) (Polysciences 23966-1) at a 2:1 ratio of PEI to DNA. Prior to transfection, DNA and PEI were each separately mixed with 250 μ L of 300 mM NaCl, vortexed, combined, and then incubated for 20 min. Transfection complexes were added dropwise to plates and cells were incubated overnight at 37°C. The following day, transfection medium was replaced with fresh medium and culture supernatant was collected at 48 and 72 h after transfection. Supernatant was centrifuged at 200×g for 5 min, filtered through a 0.45- μ m polyethersulfone (PES) membrane, and then combined with polyethylene glycol (PEG) concentrator solution (40% PEG 8000, 1.2 M sodium chloride, 1× phosphate-buffered saline [Millipore Sigma P5368]) at a ratio of 3:1 supernatant to PEG concentrator solution. Supernatant was then incubated overnight at 4°C to precipitate viral particles and centrifuged at 1500×g for 45 min. Viral pellets were resuspended in 1 mL of Dulbecco's phosphate-buffered saline (Thermo Fisher 14190250) and stored at -80°C.

Bacterial protein expression

PHIP expression constructs were transformed to Rosetta2 *E. coli* (Millipore Sigma 71403). Liquid cultures (500 mL) were grown to an OD₆₀₀ of 0.4–0.6 and induced with 0.25 mM isopropyl β -D-1-thiogalactopyranoside (IPTG) for 12 h at 18°C, pelleted by centrifugation at 3200×g, and snap-frozen in liquid nitrogen. Cells were lysed in 50 mL of lysis buffer consisting of 25 mM Tris (pH 8.0), 200 mM NaCl, 25 mM imidazole, 10% glycerol, 0.5% CHAPS, 1 mM PMSE, 0.5 mM DTT, 1× protease inhibitor (Millipore Sigma 8849), 2.5 mg/mL lysozyme, and 25 U/mL benzonase (Millipore Sigma E1014-25KU). Lysates were clarified by centrifugation at 40,000×g for 30 min. Following centrifugation, 1 mL of Ni-NTA agarose beads (Qiagen 30210) was added to the cleared supernatant and samples were incubated on a rotator for 1 h at 4°C. Ni-NTA beads were pelleted by centrifugation at 1000×g and washed three times with 50 mL of wash buffer (25 mM Tris at pH 8.0, 200 mM NaCl, 25 mM imidazole, 10% glycerol, 0.1% CHAPS). Beads were transferred into gravity flow columns (Thermo Fisher 29924) and washed twice with 5 mL of wash buffer containing 10 mM ATP and 20 mM MgCl₂, followed by two 5-mL washes with wash buffer containing 40 mM imidazole. Protein was then eluted using 5 mL of wash buffer containing 300 mM imidazole, and then concentrated/exchanged into storage buffer (20 mM Tris at pH 8.0, 200 mM NaCl, 20% glycerol, 1 mM DTT) using 10-kDa cutoff Amicon ultra filters (Millipore Sigma UFC801024 and UFC501024).

Semisynthetic nucleosomes with defined histone post-translational modifications (PTMs)

All nucleosomes in this study were from the dNuc or versaNuc portfolios (EpiCypher), with PTMs confirmed by mass

spectrometry (e.g., electrospray ionization time of flight) and immunoblotting (if an antibody was available) (Weinberg et al. 2019; Jain et al. 2020; Marunde et al. 2021).

dCypher assays

dCypher binding assays of PTM-defined Nucs (in Figs. 4, 6A–D, 7B) were performed under standard conditions that titrate Query (e.g., PHIP wild-type or mutant reader domains) to a fixed concentration of Target (e.g., PTM-defined nucleosome) (Weinberg et al. 2019; Jain et al. 2020; Marunde et al. 2021). To compare and rank targets, we used a four-parameter logistical (4PL) model to compute the relative EC₅₀ (EC₅₀^{rel}) value for each interaction (defined as the concentration of Query required to elicit a response half-way between the maximal and baseline along the concentration–dose response curve) (Marunde et al. 2021).

The interrogation of potential tripartite combinatorial engagement (Fig. 6E–H) required modified conditions and the generation of saturation curves. Here, Targets were titrated against a fixed concentration of Query. Saturation curves were executed under Target depletion/Query limited conditions, but not low enough to ensure that rapid equilibrium conditions were established (i.e., $[P] \leq 10[S]$ or $[P] \ll [S]$). This was due mainly to the limit of detection within ALPHA and the lack of a robust signal at reduced Query concentrations (i.e., <0.1 nM PHIP). To establish the saturation curve, 5 μ L of Query (e.g., 2.5 nM 6His-tagged PHIP Tudor–BD1–BD2) was incubated with 5 μ L of Target (PTM-defined nucleosome, titrated in triplicate in a 13-point/1.5-fold dilution series [10–0.077 nM final concentration] plus a buffer control [20 mM Tris-HCl at pH 7.5, 250 mM NaCl, 0.01% {w/v} BSA, 0.01% {v/v} NP-40, 1 mM DTT]) for 30 min at room temperature in a 384-well plate (PerkinElmer 6007290). A 10- μ L mix of 2.5 μ g/mL Ni-NTA AlphaLISA acceptor beads (PerkinElmer AL108) and 10 μ g/mL streptavidin AlphaScreen donor beads was added (PerkinElmer ALSU-ASDB) to each well and the plate was incubated in subdued lighting for 60 min at room temperature. AlphaLISA signal was measured on a PerkinElmer 2104 EnVision (680-nm laser excitation, 570-nm emission filter \pm 50-nm bandwidth). Data were fit to the following quadratic equation, which considers the cooperativity denoted (confirmed by examining reciprocal plots) in the saturation curves:

$$y = \left(\frac{y_{max}}{2[P]} \right) \times \left\{ K_d^h + [P] + [L]^h - \sqrt{(K_d^h + [P] + [L]^h)^2 - (4 \times [P] \times [L]^h)} \right\},$$

where P is the protein concentration in the assay, L is the ligand (nucleosome) concentration, y_{max} is the maximal signal, h is the Hill slope, and K_d is the apparent dissociation constant.

Generation of CRISPR HCT116 clones

CRISPR knockout clones were generated as described previously (Morgan et al. 2017). HCT116 cells (1×10^7) were electroporated with 30 μ g of each pX330 sgRNA plasmid along with 15 μ g of pCAGGS-EGFP-IRES-Puro. Electroporation was performed with a GenePulser Xcell equipped with PC and CE modules (Bio-Rad 1652660) using the following conditions: 200 V, 950 μ F, and infinite resistance. Following electroporation, cells were allowed to recover for 24 h and subsequently selected with 1 μ g/mL puromycin for 24 h. Four days to 5 d later, cells were seeded at 1000 cells per 10-cm dish and allowed to form single-cell-derived colonies. Colonies were picked into 96-well plates, expanded, and split into replicates. DNA from one plate was extracted with DNA lysis buffer (10 mM Tris at pH 8.5, 50 mM KCl, 1.5 mM MgCl₂,

0.45% NP-40, 0.45% Tween-20, 0.5 mg/mL proteinase K) overnight at 55°C, followed by heat inactivation of proteinase K (12 min at 95°C) and PCR amplification using Dreamtaq PCR mix (Thermo Fisher K1081).

Antibodies

Antibodies used in this study are listed in Supplemental Table 2.

Chromatin immunoprecipitation (ChIP)

ChIP was performed as described previously (Lee et al. 2006). Samples were sonicated using a Covaris E220 system. Sonication conditions were 20% duty factor for histones or 10% duty factor for nonhistone proteins, peak intensity pulse 140, and 200 cycles per burst, for 4 min.

Cell growth assay by crystal violet staining

Wild-type and BRWD TKO HCT116 cells were plated in triplicate at 6×10^5 cells/well in six-well tissue culture plates. At days 1, 2, 4, and 6 postplating, cells were fixed with 3.7% formaldehyde in PBS for 20 min, rinsed with water, and air-dried overnight. For palbociclib treatment, cells were plated at 2×10^5 cells/well in 24-well plates and then treated with 100 μ M, 10 μ M, 1 μ M, 100 nM, and 10 nM palbociclib for 72 h, at which point cells were fixed with 3.7% formaldehyde in PBS for 20 min, rinsed with water, and air-dried overnight. Fixed cells were stained with crystal violet solution (Millipore Sigma HT90132-1L) for 1 h, destained with water, and air-dried overnight. The following day, crystal violet dye was dissolved in 10% acetic acid for 1 h and then 200 μ L of each sample was measured at an optical density (OD) of 590 nm on a Tecan M1000 Pro plate reader. OD₅₉₀ values were multiplied by the volume of acetic acid used to dissolve each sample to obtain normalized OD₅₉₀ values.

Neuronal differentiation

Neuronal differentiation of mouse embryonic stem cells was as described previously (Gaspard et al. 2009).

Histone peptide microarray

Histone peptide microarrays were printed as described previously (Cornett et al. 2017). Reader hybridization and antibody-based detection were conducted as described previously (Vaughan et al. 2018). Briefly, 500 μ L of 2.5 μ M 10xHis-PHIP-Tudor–BD1–BD2-FLAG (also known as Tudor–BD1–BD2) was hybridized to histone peptide microarrays in array buffer (PBS with 5% BSA, 0.1% Tween-20) for 30 min. Bound protein was visualized by incubation with anti-FLAG (1:2000; Sigma F1804) followed by anti-mouse AlexaFluor-647 (1:5000; Invitrogen A-21235). All steps were performed at room temperature. Array was imaged by fluorescence at 20- μ m resolution (Innopsys Innoscan 1100). Data were analyzed with ArrayNinja software (Dickson et al. 2016).

RNA extraction

RNA was extracted using RNeasy RNA miniprep columns (Qiagen 74106) and subjected to on-column DNase I digestion (Qiagen 79256) according to the manufacturer's recommended protocol.

Subcellular fractionation

Cell pellets were resuspended in 6 vol of buffer 1 (10 mM HEPES-KOH at pH 7.9, 10 mM KCl, 1.5 mM MgCl₂, 340 mM sucrose, 10% glycerol, 10 mM sodium butyrate, 0.2% Triton X-100, 1× protease inhibitor cocktail [Sigma 8340]) and incubated for 10 min on ice. Samples were centrifuged at 1000×g for 5 min at 4°C. The supernatant was collected as the low-salt fraction. Pellets were resuspended in six pellet volumes of buffer A and NaCl was gradually added to 300 mM. Samples were centrifuged at 1000×g for 5 min at 4°C and the supernatant was collected as the high-salt fraction. The resulting cell pellet was resuspended in six pellet volumes of SDS sample buffer supplemented with 1 μL/mL benzonase nuclease (Millipore Sigma E1014-25KU) to solubilize chromatin.

Dithiobis(succinimidyl propionate) (DSP) cross-linking and subcellular fractionation

Flp-In T-Rex 293 cells (1 × 10⁹; Thermo Fisher R78007) expressing a FLAG-CUL4B transgene were collected by trypsinization and resuspended in 20 mL of PBS. A 250 mM stock solution of DSP (Thermo Fisher PG82081) was prepared immediately before use in anhydrous DMSO. DSP was added to cell suspensions to a final concentration of 1.25 mM (100 μL of 250 mM DSP stock to 20 mL of cell suspension) and cells were incubated for 30 min at room temperature. DSP was quenched by addition of 20 mM Tris (pH 7.5) and incubation for 15 min at room temperature. Cells were then washed three times with 20 mL of PBS and pellets were resuspended in 10 mL of lysis buffer (10 mM HEPES-KOH at pH 7.9, 10 mM KCl, 1.5 mM MgCl₂, 340 mM sucrose, 10% glycerol, 10 mM sodium butyrate, 0.25% Triton X-100, 0.5% Igepal Ca-630, 1× protease inhibitor cocktail [Sigma 8340]) and incubated for 10 min on ice. Lysates were centrifuged at 2000×g for 5 min at 4°C, the resulting supernatant was collected as the low-salt fraction, and NaCl was added to 150 mM (by addition of a 5 M NaCl stock in ~20-μL increments with mixing). The resulting pellet was resuspended in 5 mL of lysis buffer and NaCl was added to 300 mM. Samples were incubated for 10 min on ice and centrifuged at 2000×g for 5 min at 4°C. The resulting supernatant was collected as the high-salt fraction and diluted 1:1 with lysis buffer to bring the NaCl concentration to 150 mM. The resulting pellet was resuspended in 5 mL of lysis buffer and CaCl₂ was added to a concentration of 1 mM. Micrococcal nuclease (MNase) (New England Biolabs M0247S) was added to 8000 U/mL, and samples were incubated for 20 min at 37°C in a water bath. MNase digestion was terminated by addition of 2 mM EGTA and 1 mM EDTA. NaCl was then added to 150 mM and samples were incubated for 10 min on ice. Samples were then cleared by centrifugation at 20,000×g for 20 min at 4°C. To immunoprecipitate FLAG-CUL4B, 150 μL of anti-FLAG-agarose beads (Millipore Sigma A2220) was added to each fraction and samples were incubated overnight at 4°C on a rotator. Beads were washed five times with 5 mL of wash buffer (50 mM HEPES at pH 7.9, 100 mM KCl, 300 mM NaCl, 10% glycerol, 1 mM EDTA, 2 mM EGTA, 0.1% Triton X-100, 10 mM sodium butyrate) and proteins were eluted by the addition of 250 μL of elution buffer (20 mM HEPES-KOH at pH 7.9, 100 mM NaCl) containing 200 μg/mL FLAG peptide (Millipore Sigma F3290-4MG).

Mass spectrometry

Sample preparation and MS of immunoprecipitated complexes were performed as described previously (Hickox et al. 2017).

TMT mass spectrometry

Tandem mass tag MS was performed by the Thermo Fisher Scientific Center for Multiplexed Proteomics at Harvard Medical School (<http://tcmp.hms.edu>).

Next-generation sequencing processing and analysis

ChIP-seq libraries were generated with the TruSeq kit (Illumina), size selected with SPRI select beads (200–400 bp), and sequenced on an Illumina Novaseq as described previously (Morgan et al. 2017). Base calls were generated with bcl2fastq (v2.17) and read quality was assessed with FastQC (<http://www.bioinformatics.babraham.ac.uk/projects/fastqc>). ChIP-seq reads were aligned to the human genome (hg38) using Bowtie (v0.12.9) (Langmead et al. 2009), allowing two mismatches and retaining uniquely mapped reads. MACS v1.4.2 (Zhang et al. 2008) was used to call peaks using a false discovery rate filter of 0.05. Genome-wide occupancy heat maps were generated using deepTools (Ramírez et al. 2014) centered on PHIP peaks. Venn diagrams were generated using ChIPpeakAnno (Zhu et al. 2010). Sequencing data included in this study are available at Gene Expression Omnibus (GSE189235).

Competing interest statement

J.M.B., M.R.M., I.K.P., A.V., and M.-C.K. are employees of Epiccypher, a commercial developer of modified nucleosomes and supplier of reagents (e.g., PTM-defined semisynthetic nucleosomes: dNucs and versaNucs) and the dCypher nucleosome interaction assay used in this study. The other authors declare no competing interests.

Acknowledgments

Research in the Shilatfard laboratory is supported by National Institutes of Health (NIH) grant R35CA197569. Research at Epiccypher, Inc., is supported by NIH grants 2R44GM117683, 2R44CA214076, and 2R44GM116584. Research in the Rothbart laboratory is supported by NIH grant R35GM124736. R.M.V. is supported by NIH fellowship F99CA245821 from the National Cancer Institute. We thank colleagues for the kind supply of reagents (see the Material and Methods), Jeffrey N. Savas for expertise and advice in mass spectrometry analysis, Nabiha Khan for next-generation sequencing library preparation, Siddhartha Das for bioinformatics analysis, and Sanjukta Guha Thakurta for TMT MS instrumentation and analysis.

Author contributions: M.A.J.M. conceived the study, performed cellular and biochemical experiments, and wrote the manuscript. I.K.P., A.V., and M.R.M. performed dCypher assays and data analysis. J.M.B., R.W., M.J.M., and S.A.H. produced and validated PTM-defined nucleosomes. N.K. performed mass spectrometry analysis of immunoprecipitations. R.M.V. performed histone peptide microarray experiments. Z.J.D. performed subcellular fractionation experiments and immunoblotting experiments. E.J.R. generated sequencing libraries and performed Illumina sequencing. S.B.R., M.-C.K., and A.S. provided project oversight/management and input on manuscript preparation.

References

Angers S, Li T, Yi X, MacCoss MJ, Moon RT, Zheng N. 2006. Molecular architecture and assembly of the DDB1-CUL4A

- ubiquitin ligase machinery. *Nature* **443**: 590–593. doi:10.1038/nature05175
- Bezrookove V, Nosrati M, Miller JR 3rd, De Semir D, Dar AA, Vosoughi E, Vaquero E, Sucker A, Lazar AJ, Gershenwald JE, et al. 2018. Role of elevated *PHIP* copy number as a prognostic and progression marker for cutaneous melanoma. *Clin Cancer Res* **24**: 4119–4125. doi:10.1158/1078-0432.CCR-18-0791
- Bjornsson HT, Benjamin JS, Zhang L, Weissman J, Gerber EE, Chen YC, Vaurio RG, Potter MC, Hansen KD, Dietz HC. 2014. Histone deacetylase inhibition rescues structural and functional brain deficits in a mouse model of kabuki syndrome. *Sci Transl Med* **6**: 256ra135. doi:10.1126/sci translmed.3009278
- Cong L, Ran FA, Cox D, Lin S, Barretto R, Habib N, Hsu PD, Wu X, Jiang W, Marraffini LA, et al. 2013. Multiplex genome engineering using CRISPR/Cas systems. *Science* **339**: 819–823. doi:10.1126/science.1231143
- Cornett EM, Dickson BM, Rothbart SB. 2017. Analysis of histone antibody specificity with peptide microarrays. *J Vis Exp* **2017**: e55912. doi:10.3791/55912
- Cox OB, Krojer T, Collins P, Monteiro O, Talon R, Bradley A, Fedorov O, Amin J, Marsden BD, Spencer J, et al. 2016. A poised fragment library enables rapid synthetic expansion yielding the first reported inhibitors of PHIP(2), an atypical bromodomain. *Chem Sci* **7**: 2322–2330. doi:10.1039/C5SC03115J
- De Semir D, Nosrati M, Bezrookove V, Dar AA, Federman S, Bienvenu G, Venna S, Rangel J, Climent J, Meyer Tamgüney TM, et al. 2012. Pleckstrin homology domain-interacting protein (PHIP) as a marker and mediator of melanoma metastasis. *Proc Natl Acad Sci* **109**: 7067–7072. doi:10.1073/pnas.1119949109
- de Semir D, Bezrookove V, Nosrati M, Dar AA, Wu C, Shen J, Rieken C, Venkatasubramanian M, Miller JR 3rd, Desprez PY, et al. 2018. PHIP as a therapeutic target for driver-negative subtypes of melanoma, breast, and lung cancer. *Proc Natl Acad Sci* **115**: E5766–E5775. doi:10.1073/pnas.1804779115
- de Semir D, Bezrookove V, Nosrati M, Scanlon KR, Singer E, Judkins J, Rieken C, Wu C, Shen J, Schmudermayer C, et al. 2020. PHIP drives glioblastoma motility and invasion by regulating the focal adhesion complex. *Proc Natl Acad Sci* **117**: 9064–9073. doi:10.1073/pnas.1914505117
- Dickson BM, Cornett EM, Ramjan Z, Rothbart SB. 2016. Array-Ninja: an open source platform for unified planning and analysis of microarray experiments. *Methods Enzymol* **574**: 53–77. doi:10.1016/bs.mie.2016.02.002
- Dilworth D, Hanley RP, Ferreira de Freitas R, Allali-Hassani A, Zhou M, Mehta N, Marunde MR, Ackloo S, Machado RAM, Yazdi AK, et al. 2021. Pharmacological targeting of a PWWP domain demonstrates cooperative control of NSD2 localization. *Nat Chem Biol* doi:10.1038/s41589-021-00898-0.
- Field M, Tarpey PS, Smith R, Edkins S, O'Meara S, Stevens C, Tofts C, Teague J, Butler A, Dicks E, et al. 2007. Mutations in the *BRWD3* gene cause X-linked mental retardation associated with macrocephaly. *Am J Hum Genet* **81**: 367–374. doi:10.1086/520677
- Filippakopoulos P, Picaud S, Mangos M, Keates T, Lambert JP, Barsyte-Lovejoy D, Felletar I, Volkmer R, Müller S, Pawson T, et al. 2012. Histone recognition and large-scale structural analysis of the human bromodomain family. *Cell* **149**: 214–231. doi:10.1016/j.cell.2012.02.013
- Firth HV, Richards SM, Bevan AP, Clayton S, Corpas M, Rajan D, Vooren SV, Moreau Y, Pettett RM, Carter NP. 2009. DECIPHER: database of chromosomal imbalance and phenotype in humans using Ensembl resources. *Am J Hum Genet* **84**: 524–533. doi:10.1016/j.ajhg.2009.03.010
- Flynn EM, Huang OW, Poy F, Oppikofer M, Bellon SF, Tang Y, Cochran AG. 2015. A subset of human bromodomains recognizes butyryllysine and crotonyllysine histone peptide modifications. *Structure* **23**: 1801–1814. doi:10.1016/j.str.2015.08.004
- Gaspard N, Bouschet T, Herpoel A, Naeije G, van den Ameele J, Vanderhaeghen P. 2009. Generation of cortical neurons from mouse embryonic stem cells. *Nat Protoc* **4**: 1454–1463. doi:10.1038/nprot.2009.157
- He YJ, McCall CM, Hu J, Zeng Y, Xiong Y. 2006. DDB1 functions as a linker to recruit receptor WD40 proteins to CUL4–ROC1 ubiquitin ligases. *Genes Dev* **20**: 2949–2954. doi:10.1101/gad.1483206
- Hickox AE, Wong AC, Pak K, Strojny C, Ramirez M, Yates JR 3rd, Ryan AF, Savas JN. 2017. Global analysis of protein expression of inner ear hair cells. *J Neurosci* **37**: 1320–1339. doi:10.1523/JNEUROSCI.2267-16.2016
- Higa LA, Wu M, Ye T, Kobayashi R, Sun H, Zhang H. 2006. CUL4–DDB1 ubiquitin ligase interacts with multiple WD40-repeat proteins and regulates histone methylation. *Nat Cell Biol* **8**: 1277–1283. doi:10.1038/ncb1490
- Hu J, Zacharek S, He YJ, Lee H, Shumway S, Duronio RJ, Xiong Y. 2008. WD40 protein FBW5 promotes ubiquitination of tumor suppressor TSC2 by DDB1–CUL4–ROC1 ligase. *Genes Dev* **22**: 866–871. doi:10.1101/gad.1624008
- Jacobson RH, Ladurner AG, King DS, Tjian R. 2000. Structure and function of a human TAF_{II}250 double bromodomain module. *Science* **288**: 1422–1425. doi:10.1126/science.288.5470.1422
- Jain K, Fraser CS, Marunde MR, Parker MM, Sagum C, Burg JM, Hall N, Popova IK, Rodriguez KL, Vaidya A, et al. 2020. Characterization of the plant homeodomain (PHD) reader family for their histone tail interactions. *Epigenetics Chromatin* **13**: 3. doi:10.1186/s13072-020-0328-z
- Jang SM, Zhang Y, Utani K, Fu H, Redon CE, Marks AB, Smith OK, Redmond CJ, Baris AM, Tulchinsky DA, et al. 2018. The replication initiation determinant protein (RepID) modulates replication by recruiting CUL4 to chromatin. *Nat Commun* **9**: 2782. doi:10.1038/s41467-018-05177-6
- Jang SM, Nathans JF, Fu H, Redon CE, Jenkins LM, Thakur BL, Pongor LS, Baris AM, Gross JM, O'Neill MJ, et al. 2020. The RepID–CRL4 ubiquitin ligase complex regulates metaphase to anaphase transition via BUB3 degradation. *Nat Commun* **11**: 24. doi:10.1038/s41467-019-13808-9
- Jansen S, Hoischen A, Coe BP, Carvill GL, Van Esch H, Bosch DGM, Andersen UA, Baker C, Bauters M, Bernier RA, et al. 2018. A genotype-first approach identifies an intellectual disability-overweight syndrome caused by PHIP haploinsufficiency. *Eur J Hum Genet* **26**: 54–63. doi:10.1038/s41431-017-0039-5
- Jin J, Arias EE, Chen J, Harper JW, Walter JC. 2006. A family of diverse Cul4–Ddb1-interacting proteins includes Cdt2, which is required for S phase destruction of the replication factor Cdt1. *Mol Cell* **23**: 709–721. doi:10.1016/j.molcel.2006.08.010
- Kouzarides T. 2007. Chromatin modifications and their function. *Cell* **128**: 693–705. doi:10.1016/j.cell.2007.02.005
- Kueh AJ, Eccles S, Tang L, Garnham AL, May RE, Herold MJ, Smyth GK, Voss AK, Thomas T. 2020. HBO1 (KAT7) does not have an essential role in cell proliferation, DNA replication, or histone 4 acetylation in human cells. *Mol Cell Biol* **40**: e00506–e00519. doi:10.1128/MCB.00506-19
- Langmead B, Trapnell C, Pop M, Salzberg SL. 2009. Ultrafast and memory-efficient alignment of short DNA sequences to the

- human genome. *Genome Biol* **10**: R25. doi:10.1186/gb-2009-10-3-r25
- Lee KK, Workman JL. 2007. Histone acetyltransferase complexes: one size doesn't fit all. *Nat Rev Mol Cell Biol* **8**: 284–295. doi:10.1038/nrm2145
- Lee TJ, Johnstone SE, Young RA. 2006. Chromatin immunoprecipitation and microarray-based analysis of protein location. *Nat Protoc* **1**: 729–748. doi:10.1038/nprot.2006.98
- Li S, Francisco AB, Han C, Pattabiraman S, Foote MR, Giesy SL, Wang C, Schimenti JC, Boisclair YR, Long Q. 2010. The full-length isoform of the mouse pleckstrin homology domain-interacting protein (PHIP) is required for postnatal growth. *FEBS Lett* **584**: 4121–4127. doi:10.1016/j.febslet.2010.08.042
- Li N, Li Y, Lv J, Zheng X, Wen H, Shen H, Zhu G, Chen TY, Dhar SS, Kan PY, et al. 2016. ZMYND8 reads the dual histone mark H3K4me1-H3K14ac to antagonize the expression of metastasis-linked genes. *Mol Cell* **63**: 470–484. doi:10.1016/j.molcel.2016.06.035
- Lydeard JR, Schulman BA, Harper JW. 2013. Building and remodeling Cullin–RING E3 ubiquitin ligases. *EMBO Rep* **14**: 1050–1061. doi:10.1038/embor.2013.173
- Mandal M, Hamel KM, Maienschein-Cline M, Tanaka A, Teng G, Tuteja JH, Bunker JJ, Bahroos N, Eppig JJ, Schatz DG, et al. 2015. Histone reader BRWD1 targets and restricts recombination to the Igk locus. *Nat Immunol* **16**: 1094–1103. doi:10.1038/ni.3249
- Marenne G, Hendricks AE, Perdikari A, Bounds R, Payne F, Keogh JM, Lelliott CJ, Henning E, Pathan S, Ashford S, et al. 2020. Exome sequencing identifies genes and gene sets contributing to severe childhood obesity, linking PHIP variants to repressed POMC transcription. *Cell Metab* **31**: 1107–1119.e12. doi:10.1016/j.cmet.2020.05.007
- Marunde MR, Popova IK, Weinzapfel EN, Keogh M-C. 2021. The dCypher approach to interrogate chromatin reader activity against PTM-defined histone peptides and nucleosomes. *Methods Mol Biol* (in press).
- McLeod C, Gout AM, Zhou X, Thrasher A, Rahbarinia D, Brady SW, Macias M, Birch K, Finkelstein D, Sunny J, et al. 2021. St. jude cloud-a pediatric cancer genomic data sharing ecosystem. *Cancer Discov* **11**: 1082–1099. doi:10.1158/2159-8290.CD-20-1230
- Morgan MAJ, Shilatifard A. 2020. Reevaluating the roles of histone-modifying enzymes and their associated chromatin modifications in transcriptional regulation. *Nat Genet* **52**: 1271–1281. doi:10.1038/s41588-020-00736-4
- Morgan MAJ, Rickels RA, Collings CK, He X, Cao K, Herz HM, Cozzolino KA, Abshiru NA, Marshall SA, Rendleman EJ, et al. 2017. A cryptic tudor domain links BRWD2/PHIP to COMPASS-mediated histone H3K4 methylation. *Genes Dev* **31**: 2003–2014. doi:10.1101/gad.305201.117
- Musselman CA, Lalonde M-E, Côté J, Kutateladze TG. 2012. Perceiving the epigenetic landscape through histone readers. *Nat Struct Mol Biol* **19**: 1218–1227. doi:10.1038/nsmb.2436
- Petroski MD, Deshaies RJ. 2005. Function and regulation of cullin–RING ubiquitin ligases. *Nat Rev Mol Cell Biol* **6**: 9–20. doi:10.1038/nrm1547
- Philipps DL, Wigglesworth K, Hartford SA, Sun F, Pattabiraman S, Schimenti K, Handel M, Eppig JJ, Schimenti JC. 2008. The dual bromodomain and WD repeat-containing mouse protein BRWD1 is required for normal spermiogenesis and the oocyte-embryo transition. *Dev Biol* **317**: 72–82. doi:10.1016/j.ydbio.2008.02.018
- Picaud S, Fedorov O, Thanasopoulou A, Leonards K, Jones K, Meier J, Olzscha H, Monteiro O, Martin S, Philpott M, et al. 2015. Generation of a selective small molecule inhibitor of the CBP/p300 bromodomain for leukemia therapy. *Cancer Res* **75**: 5106–5119. doi:10.1158/0008-5472.CAN-15-0236
- Ramírez F, Dündar F, Diehl S, Grüning BA, Manke T. 2014. DeepTools: a flexible platform for exploring deep-sequencing data. *Nucleic Acids Res* **42**: W187–W191. doi:10.1093/nar/gku365
- Reitsma JM, Liu X, Reichermeier KM, Moradian A, Sweredoski MJ, Hess S, Deshaies RJ. 2017. Composition and regulation of the cellular repertoire of SCF ubiquitin ligases. *Cell* **171**: 1326–1339.e14. doi:10.1016/j.cell.2017.10.016
- Roth SY, Denu JM, Allis CD. 2001. Histone acetyltransferases. *Annu Rev Biochem* **70**: 81–120. doi:10.1146/annurev.biochem.70.1.81
- Ruthenburg AJ, Li H, Patel DJ, Allis CD. 2007. Multivalent engagement of chromatin modifications by linked binding modules. *Nat Rev Mol Cell Biol* **8**: 983–994. doi:10.1038/nrm2298
- Savitsky P, Krojer T, Fujisawa T, Lambert JP, Picaud S, Wang CY, Shanle EK, Krajewski K, Friedrichsen H, Kanapin A, et al. 2016. Multivalent histone and DNA engagement by a PHD/BRD/PWWP triple reader cassette recruits ZMYND8 to K14ac-rich chromatin. *Cell Rep* **17**: 2724–2737. doi:10.1016/j.celrep.2016.11.014
- Tarpey PS, Raymond FL, O'Meara S, Edkins S, Teague J, Butler A, Dicks E, Stevens C, Tofts C, Avis T, et al. 2007. Mutations in CUL4B, which encodes a ubiquitin E3 ligase subunit, cause an X-linked mental retardation syndrome associated with aggressive outbursts, seizures, relative macrocephaly, central obesity, hypogonadism, pes cavus, and tremor. *Am J Hum Genet* **80**: 345–352. doi:10.1086/511134
- Tate JG, Bamford S, Jubb HC, Sondka Z, Beare DM, Bindal N, Boutselakis H, Cole CG, Creatore C, Dawson E, et al. 2019. COSMIC: the catalogue of somatic mutations in cancer. *Nucleic Acids Res* **47**: D941–D947. doi:10.1093/nar/gky1015
- Tenorio J, Alarcón P, Arias P, Ramos FJ, Campistol J, Climent S, García-Miñaur S, Dapía I, Hernández A, Nevado J, et al. 2019. MRX93 syndrome (BRWD3 gene): five new patients with novel mutations. *Clin Genet* **95**: 726–731. doi:10.1111/cge.13504
- Townsend A, Lora G, Engel J, Tirado-Class N, Dungrawala H. 2021. DCAF14 promotes stalled fork stability to maintain genome integrity. *Cell Rep* **34**: 108669. doi:10.1016/j.celrep.2020.108669
- van der Donk R, Jansen S, Schuurs-Hoeijmakers JHM, Koolen DA, Goltstein LCMJ, Hoischen A, Brunner HG, Kemmeren P, Nellåker C, Vissers LELM, et al. 2019. Next-generation phenotyping using computer vision algorithms in rare genomic neurodevelopmental disorders. *Genet Med* **21**: 1719–1725. doi:10.1038/s41436-018-0404-y
- Vaughan RM, Dickson BM, Cornett EM, Harrison JS, Kuhlman B, Rothbart SB. 2018. Comparative biochemical analysis of UHRF proteins reveals molecular mechanisms that uncouple UHRF2 from DNA methylation maintenance. *Nucleic Acids Res* **46**: 4405–4416. doi:10.1093/nar/gky151
- Wang L, Shilatifard A. 2019. UTX mutations in human cancer. *Cancer Cell* **35**: 168–176. doi:10.1016/j.ccell.2019.01.001
- Weber J, de la Rosa J, Grove CS, Schick M, Rad L, Baranov O, Strong A, Pfaus A, Friedrich MJ, Engleitner T, et al. 2019. Piggybac transposon tools for recessive screening identify B-cell lymphoma drivers in mice. *Nat Commun* **10**: 1415. doi:10.1038/s41467-019-09180-3
- Webster E, Cho MT, Alexander N, Desai S, Naidu S, Bekheirnia MR, Lewis A, Retterer K, Juusola J, Chung WK. 2016. De novo PHIP-predicted deleterious variants are associated with developmental delay, intellectual disability, obesity, and dysmorphic features. *Cold Spring Harb Mol Case Stud* **2**: a001172. doi:10.1101/mcs.a001172

- Wei J, Alfajaro MM, DeWeirdt PC, Hanna RE, Lu-Culligan WJ, Cai WL, Strine MS, Zhang SM, Graziano VR, Schmitz CO, et al. 2020. Genome-wide CRISPR screens reveal host factors critical for SARS-CoV-2 infection. *Cell* **184**: 76–91.e13. doi:10.1016/j.cell.2020.10.028
- Weinberg DN, Papillon-Cavanagh S, Chen H, Yue Y, Chen X, Rajagopalan KN, Horth C, McGuire JT, Xu X, Nikbakht H, et al. 2019. The histone mark H3K36me2 recruits DNMT3A and shapes the intergenic DNA methylation landscape. *Nature* **573**: 281–286. doi:10.1038/s41586-019-1534-3
- Yu J, Vodyanik MA, Smuga-Otto K, Antosiewicz-Bourget J, Frane JL, Tian S, Nie J, Jonsdottir GA, Ruotti V, Stewart R, et al. 2007. Induced pluripotent stem cell lines derived from human somatic cells. *Science* **318**: 1917–1920. doi:10.1126/science.1151526
- Zeng L, Yap KL, Ivanov AV, Wang X, Mujtaba S, Plotnikova O, Rauscher FJ 3rd, Zhou MM. 2008. Structural insights into human KAP1 PHD finger-bromodomain and its role in gene silencing. *Nat Struct Mol Biol* **15**: 626–633. doi:10.1038/nsmb.1416
- Zhang Y, Liu T, Meyer CA, Eeckhoutte J, Johnson DS, Bernstein BE, Nusbaum C, Myers RM, Brown M, Li W, et al. 2008. Model-based analysis of ChIP-seq (MACS). *Genome Biol* **9**: R137. doi:10.1186/gb-2008-9-9-r137
- Zhang Y, Huang L, Fu H, Smith OK, Lin CM, Utani K, Rao M, Reinhold WC, Redon CE, Ryan M, et al. 2016. A replicator-specific binding protein essential for site-specific initiation of DNA replication in mammalian cells. *Nat Commun* **7**: 11748. doi:10.1038/ncomms11748
- Zhang L, Pilarowski G, Pich EM, Nakatani A, Dunlop J, Baba R, Matsuda S, Daini M, Hattori Y, Matsumoto S, et al. 2021. Inhibition of KDM1A activity restores adult neurogenesis and improves hippocampal memory in a mouse model of Kabuki syndrome. *Mol Ther Methods Clin Dev* **20**: 779–791. doi:10.1016/j.omtm.2021.02.011
- Zhu LJ, Gazin C, Lawson ND, Pagès H, Lin SM, Lapointe DS, Green MR. 2010. ChIPpeakAnno: a Bioconductor package to annotate ChIP-seq and ChIP-chip data. *BMC Bioinformatics* **11**: 237. doi:10.1186/1471-2105-11-237
- Zou Y, Liu Q, Chen B, Zhang X, Guo C, Zhou H, Li J, Gao G, Guo Y, Yan C, et al. 2007. Mutation in CUL4B, which encodes a member of cullin-RING ubiquitin ligase complex, causes X-linked mental retardation. *Am J Hum Genet* **80**: 561–566. doi:10.1086/512489